Journal of Materials Chemistry B

ROYAL SOCIETY OF CHEMISTRY

PAPER

View Article Online
View Journal | View Issue

Cite this: J. Mater. Chem. B, 2020, 8, 3038

Integrating silicon/zinc dual elements with PLGA microspheres in calcium phosphate cement scaffolds synergistically enhances bone regeneration

Weiwei Liang,†[abc] Min Gao,†[a] Jingsheng Lou,[d] Yunyang Bai,[a] Jing Zhang,[e] Teliang Lu,[e] Xiaowen Sun,[c] Jiandong Ye,[e] Baowei Li,[d] Li Sun,*[d] Boon Chin Heng,*[f] Xuehui Zhang *[cg] and Xuliang Deng[ag]

Integrating multiple pro-osteogenic factors into bone graft substitutes is a practical and effective approach to improve bone repair efficacy. Here, Si–Zn dual elements and PLGA microspheres were incorporated into calcium phosphate cement (CPC) scaffolds (PLGA/CPC-Si/Zn) as a novel strategy to synergistically enhance bone regeneration. The incorporation of PLGA microspheres and Si/Zn dual elements within CPC scaffolds improved the setting time, injectability and compressive strength. The PLGA/CPC-Si/Zn scaffolds displayed controlled sequential release of Si and Zn ions. *In vitro*, RAW 264.7 cells displayed the M2 phenotype with a high level of anti-inflammatory cytokines in response to PLGA/CPC-Si/Zn. The conditioned medium of RAW 264.7 cells cultured on the PLGA/CPC-Si/Zn scaffolds significantly enhanced the osteogenic differentiation of rat BMSCs. In a rat femur defect model, the implanted PLGA/CPC-Si/Zn scaffolds led to obvious new bone formation after 4 weeks, apparent bone ingrowth into the PLGA microspheres after 12 weeks, and was almost completely filled with mature new bone upon degradation of the PLGA microspheres at 24 weeks. These findings demonstrate that the PLGA/CPC-Si/Zn scaffolds promote osteogenesis by synergistically improving the immune microenvironment and biodegradability. Hence, integrating multiple trace elements together with degradable components within bone graft biomaterials can be an effective strategy for promoting bone regeneration.

Received 21st December 2019,
Accepted 10th March 2020

DOI: 10.1039/c9tb02901j

rsc.li/materials-b

1. Introduction

Biomaterial scaffolds play a critical role in bone defect repair by serving as artificial extracellular matrices that present both chemical and physical cues for modulating osteoconductive effects and degradation to provide space for new bone ingrowth and to promote vascularization.[1,2] However, approaches that allow us to build devices integrating these cues in a combinatorial way are limited due to the lack of suitable component materials and appropriate manufacturing processes.

Numerous reports have confirmed that doping of biomaterials with trace elements such as silicon (Si), zinc (Zn), magnesium (Mg), strontium (Sr) and iron (Fe) can significantly enhance osteogenesis of calcium phosphate scaffolds[3,4] *i.e.* calcium phosphate cement (CPC). Doping biomaterials with more than one trace element is considered a viable approach mimicking the natural physiological extracellular environment in which multiple trace elements are present to facilitate osteogenesis.[5] Different elements play different roles in the bone regeneration process. For example, Si can promote vascularization and collagen synthesis,[6,7] while zinc can stimulate bone growth and mineralization, increase osteoblast activity and inhibit osteoclast activity.[8] The ability of multiple element incorporation to functionally coordinate with the natural bone regeneration process provides a novel strategy for biomaterial development.[9]

[a] Department of Geriatric Dentistry, Peking University School and Hospital of Stomatology, Beijing 100081, P. R. China
[b] Department of Prosthodonitcs, Peking University School and Hospital of Stomatology, Beijing 10081, P. R. China
[c] Department of Dental Materials & Dental Medical Devices Testing Centre, Peking University School and Hospital of Stomatology, Beijing 100081, P. R. China. E-mail: zhangxuehui@bjmu.edu.cn
[d] Anesthesia and Operation Centre, Chinese PLA General Hospital, Beijing 410078, P. R. China. E-mail: 13501091260@163.com
[e] School of Materials Science and Engineering, South China University of Technology, Guangzhou 510641, China
[f] Central Laboratory, Peking University School and Hospital of Stomatology, Beijing 100081, P. R. China. E-mail: hengboonchin@bjmu.edu.cn
[g] National Engineering Laboratory for Digital and Material Technology of Stomatology, NMPA Key Laboratory for Dental Materials & Beijing Laboratory of Biomedical Materials, Peking University School and Hospital of Stomatology, Beijing 100081, P. R. China
† These authors contributed equally to this work.

Trace elements have also been reported to play a pivotal role in bone biomaterial-stimulated osteogenesis through immunomodulation.[10–12] Trace element doped CPC scaffolds can effectively regulate the macrophage M1/M2 phenotype transition, thereby promoting bone regeneration and repair.[13] Studies to date have tended to focus mainly on single trace elements, and the effects of co-doping biomaterials with multiple trace elements on the immune response of macrophages remain unclear.

Poor biodegradability and lack of an internal bone germinal center, usually compromise the bone repair efficacy of CPC scaffolds.[14,15] In order to overcome these shortcomings, Ye *et al.* has investigated the use of poly(lactic-*co*-glycolic acid) (PLGA) microspheres to improve the biodegradability of CPC, which facilitates macropore formation conducive for cell ingrowth *in situ*, as well as enable the possible controlled release of bioactive factors during the degradation process.[16] The incorporated PLGA microspheres can provide the required high mechanical strength to CPC scaffolds during the early stage of bone repair, and gradually degrade to create macropores for bone ingrowth.[17] The synergistic effects of incorporating multiple elements and PLGA microspheres in enhancing bone regeneration is a major consideration in our CPC scaffold design. How the elemental release kinetics and PLGA microspheres degradation of the CPC scaffold is synchronized to match the developmental timescale of bone regeneration is of great interest, and remains a major challenge for bone regeneration applications.

Hence, this study aimed to integrate the synergistic effects of Si/Zn dual-element and PLGA microsphere incorporation within CPC scaffolds to modulate macrophage immune response and bone defect repair (Fig. 1). The physicochemical properties including setting time, injectability, compressive strength, porosity and ion release behavior of PLGA/CPC scaffolds incorporated with different trace elements were characterized. The immune responses of macrophages to Si/Zn incorporated PLGA/CPC scaffolds, including cell morphology, M1/M2 phenotypic transition and inflammatory factor secretion were evaluated. Finally, the osteogenic differentiation of rat bone marrow mesenchymal stem cells (BMSCs) in the presence of macrophage conditioned-medium *in vitro* and efficacy of the implanted Si/Zn dual element incorporated PLGA/CPC (PLGA/CPC-Si/Zn) scaffolds in promoting bone regeneration *in situ* within a rat femur critical-size defect model were investigated.

2. Results

2.1 Physicochemical properties of PLGA/CPC-Si/Zn scaffolds synthetic procedures

The cross-sectional SEM imaging showed that the hollow PLGA microspheres with sizes ranging 50–200 μm were uniformly embedded within the scaffold without aggregation (Fig. 2A). The outer walls of the microspheres contacted tightly with the scaffold matrix without interface separation. The incorporation of trace elements did not affect the uniform distribution of PLGA microspheres. The phase composition of materials was determined by X-ray diffraction as presented in Fig. 2B. For all scaffolds utilized in this study, the characteristic peaks of hydroxyapatite (HA), which were hydration products of CPC, could be clearly seen in the XRD patterns. There was no anhydrous dicalcium phosphate (DCPA, $CaHPO_4$), which indicated completion of the DCPA reaction in the raw material. Zinc pyrophosphate ($Zn_2P_2O_7$) was detected in the PLGA/CPC-Zn scaffolds. Other components of the scaffolds were not shown in the XRD map because of the different doping forms of trace elements and determination limitation (5%) of XRD. Energy-dispersive spectroscopy (EDS) (Fig. 2C) showed the distribution of trace elements Ca (color green), P (color blue), Zn (color orange) and Si (color yellow) in the PLGA/CPC-Si/Zn scaffolds.

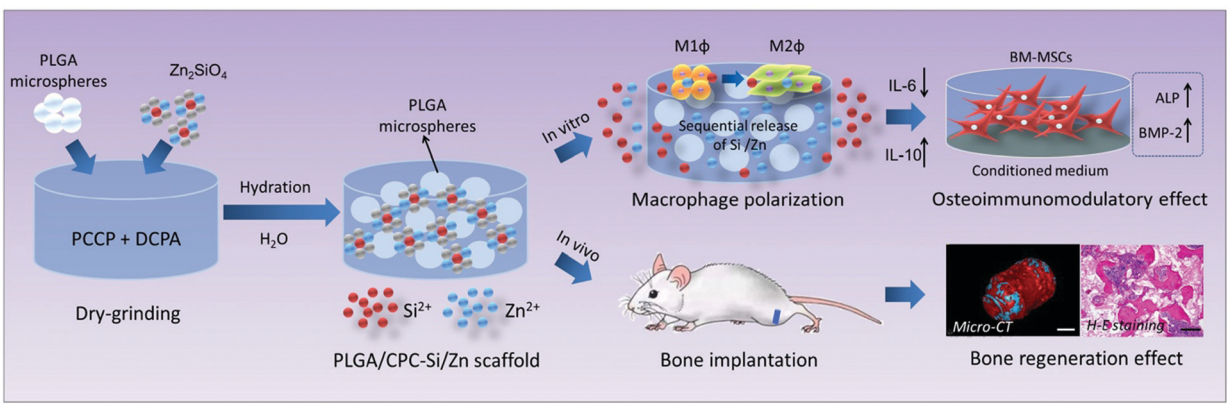

Fig. 1 Schematic illustration of silicon–zinc doped PLGA/CPC scaffolds promoting bone regeneration. Schematic illustration of silicon–zinc doped PLGA/CPC scaffolds promoting bone regeneration. Silicon–zinc (Si/Zn) dual-elements were incorporated into the calcium phosphate cement (CPC) scaffolds together with loading of PLGA microspheres. *In vitro*, RAW 264.7 cells (macrophages) displayed a trend towards the M2 phenotype and expressed low levels of pro-inflammatory factor IL-6 and high levels of anti-inflammatory gene IL-10. Moreover, the RAW 264.7 cell conditioned medium of PLGA/CPC-Si/Zn significantly enhanced the osteogenic capacity of rat BMSCs, which expressed high levels of BMP-2. *In vivo*, upon implantation of PLGA/CPC-Si/Zn scaffolds into a rat femur defect model, significant new bone formation was observed at the center of the scaffold after 4 weeks, as shown by micro-CT analysis, and there was mature bone tissue ingrowth into the PLGA microspheres after 24 weeks, as shown by the H–E staining image, thus suggesting that CPC scaffolds doped with dual-elements exhibit osteoimmunomodulatory effects that promote bone regeneration.

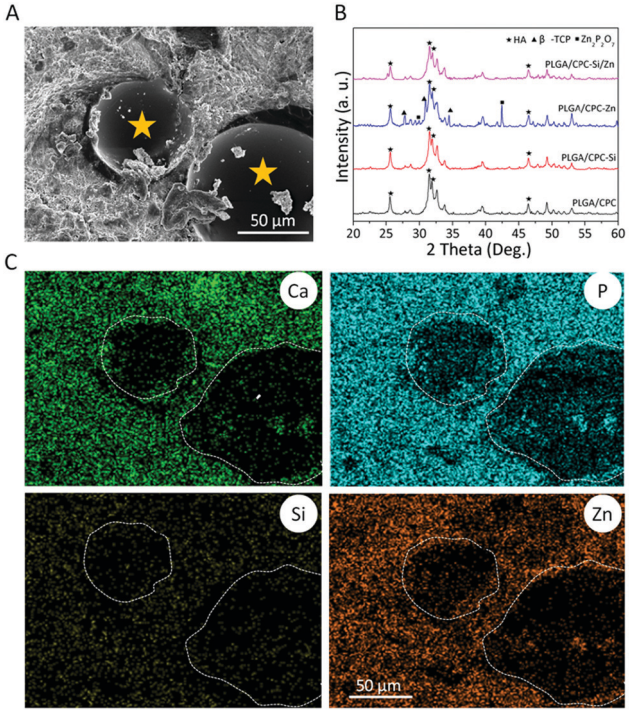

Fig. 2 Structure and composition of Si/Zn dual-element incorporated PLGA/CPC scaffolds. (A) SEM images of Si/Zn co-incorporated PLGA/CPC scaffold materials. Yellow pentagrams denote PLGA microspheres. (B) X-ray diffraction patterns of PLGA/CPC-based materials. (C) EDS spectra of the distribution of elements within PLGA/CPC-Si/Zn scaffold. Dotted lines denote PLGA microspheres.

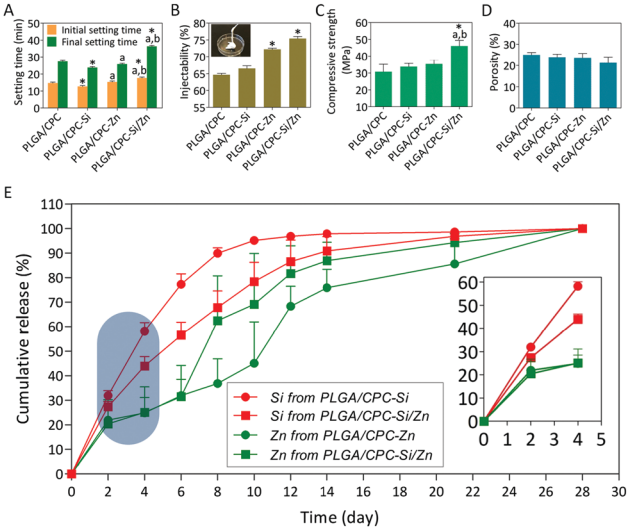

Fig. 3 Physicochemical properties and ion release profiles of PLGA/CPC-based scaffolds. (A) The setting time. (B) The injectability and injection schematic is shown in the inset. (C) The porosity. (D) The compressive strength. (E) Cumulative percentage release of ions from different scaffolds during 28 days. Inset shows the first 4 days of release. *Indicates statistically significant difference ($p < 0.05$) compared to the PLGA/CPC group. Statistically significant differences between other groups are indicated with letters (a and b) where 'a' and 'b' indicate significant difference ($p < 0.05$) compared to PLGA/CPC-Si and PLGA/CPC-Zn respectively.

As shown in Fig. 3A, the initial setting time of the PLGA/CPC scaffold without trace element doping was 15 min and its final setting time was about 27 min. The incorporation of Zn element did not significantly change the setting time of the PLGA/CPC scaffold, while the incorporation of Si element shortened the setting time. Interestingly, the incorporation of Si and Zn dual-elements significantly prolonged both the initial setting time (17 min) and final setting time (36 min). The injectability was next investigated, as shown in Fig. 3B. The injectability was about 64% for PLGA/CPC scaffold and it tended to increase upon doping with trace elements, particularly in the case of PLGA/CPC-Si/Zn, possessing an injectability of about 75%, which was useful for clinical practice. The incorporation of trace elements can improve the compressive strength of the PLGA/CPC scaffold (Fig. 3C). The compressive strength value was about 30 MPa for the PLGA/CPC scaffold and it increased with incorporated trace elements, particularly in the case of the PLGA/CPC-Si/Zn scaffold, which possessed a compressive strength value up to 45 MPa. Bone substitute materials with high strength are required for maintaining the environment of bone defects undergoing the repair process and to provide space for new bone growth.[18] The porosity of all kinds of scaffolds are shown in Fig. 3D. There were no significant differences between all groups and the porosity ranged between 20% and 25%, indicating that incorporation with trace elements did not influence porosity of the PLGA/CPC scaffold.

2.2 Ion release profile of PLGA/CPC-Si/Zn scaffolds

The release kinetics of trace elements are presented in Fig. 3E. Generally, the release of Si and Zn ions from scaffolds showed an initial burst release behavior, particularly the rapid release behavior of Si in the PLGA/CPC-Si group which continued until the 8th day, and then gradually reached a sustained release state. The Si ion was released faster than the Zn ion in either the single-element incorporated group or the dual-element incorporated group. As compared to the PLGA/CPC-Si group, the PLGA/CPC-Si/Zn group released Si at a relatively slower rate, with both groups reaching saturation point by day 21. The PLGA/CPC-Si/Zn group released Zn at a relatively faster rate than the PLGA/CPC-Zn group from day 6 onwards, with both groups reaching saturation point by day 28. It can be seen from the two-element incorporated group that Si and Zn exhibit a sequential release profile for at least 2 weeks, which might have a certain biological significance.

2.3 Immunomodulatory effects through interaction of macrophages with PLGA/CPC-Si/Zn scaffolds

RAW 264.7 cells, a typical representative *in vitro* model of innate immunity, were utilized in this study to investigate regulation of the immune response by the PLGA/CPC-Si/Zn scaffolds. Initially, RAW 264.7 cells seeded on the various scaffolds exhibited a small and rounded morphology on the first day (Fig. 4A). Quantitative analysis showed that the PLGA/CPC-Si/Zn group displayed the largest cell spreading area, while the aspect ratio was not significantly different between groups (Fig. 4B). These implied that dual-element-incorporated scaffolds could enhance macrophage

adhesion and spreading compared to single- or non-incorporated scaffolds. On the third day, macrophages cultured on the trace element incorporated scaffolds appeared much narrower and more elongated, as compared to cells of the non-incorporated scaffolds, which more closely-resembled the typical morphology of the anti-inflammatory M2 phenotype, according to previous studies.[19,20] In particular, the dual-element incorporated scaffold group displayed the largest cell elongation ratio, which implied their most potent anti-inflammatory effects, as compared to single-element incorporated or non-incorporated scaffolds (Fig. 4C). Consistently, stimulation of RAW 264.7 cells with the PLGA/CPC-Si/Zn scaffold resulted in a shift towards the M2 phenotype, with most cells expressing the surface marker CD206, as compared to cells stimulated with other scaffolds (Fig. 5A). By contrast, the same treatment resulted in the least cells expressing the pro-inflammatory surface marker CCR7 in the PLGA/CPC-Si/Zn scaffold group, as compared to the single-element incorporated or non-incorporated scaffold group (Fig. 5A).

For inflammatory gene expression, the RAW macrophages seeded on the PLGA/CPC-Si/Zn scaffold displayed significantly lower pro-inflammatory gene TNF-α expression and higher anti-inflammatory IL-10 and TGF-1β expression levels, as compared to either the PLGA/CPC-Si or PLGA/CPC-Zn groups on day 3 ($p < 0.05$) (Fig. 5B). ELISA results showed that the pro-inflammatory factor IL-6 secreted by RAW macrophages on dual-element incorporated scaffold was at the lowest level amongst all groups from day 1 to day 3 (Fig. 5C). These results demonstrated that after stimulation with the PLGA/CPC-Si/Zn scaffold for 3 days, the RAW cells displayed a trend towards the M2 phenotype. In addition, there were significantly higher expression levels of vascular genes VEGF and PDGF-BB in the PLGA/CPC-Si/Zn group, as compared to the other three groups on day 3 ($P < 0.05$) (Fig. 5D).

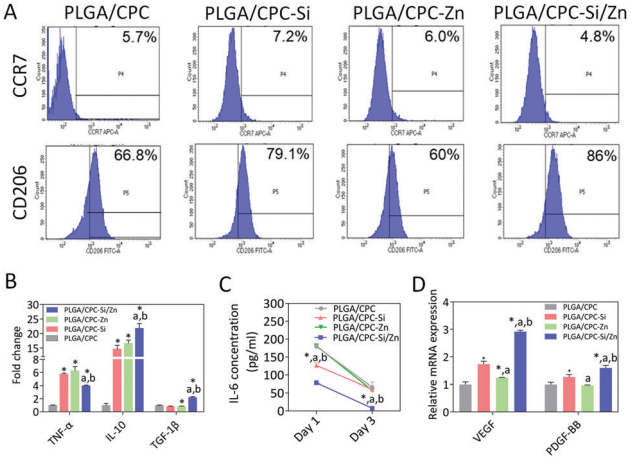

Fig. 5 Immunomodulatory effects through interaction of macrophages with PLGA/CPC-based scaffolds. (A) FACS analysis of RAW 264.7 cells stimulated by the various scaffold materials on day 3. (B) mRNA expression levels of inflammatory gene markers within RAW 264.7 cells cultured on different PLGA/CPC materials on day 3. (C) Cytokine expression of IL-6 from day 1 to day 3 detected by ELISA. (D) mRNA expression levels of vascular gene markers within RAW 264.7 cells cultured on different PLGA/CPC materials on day 3. * Indicates statistically significant difference ($p < 0.05$) compared to the PLGA/CPC group. Statistically significant differences between other groups are indicated with letters (a and b) where 'a' and 'b' indicate significant difference ($p < 0.05$) compared to PLGA/CPC-Si and PLGA/CPC-Zn respectively.

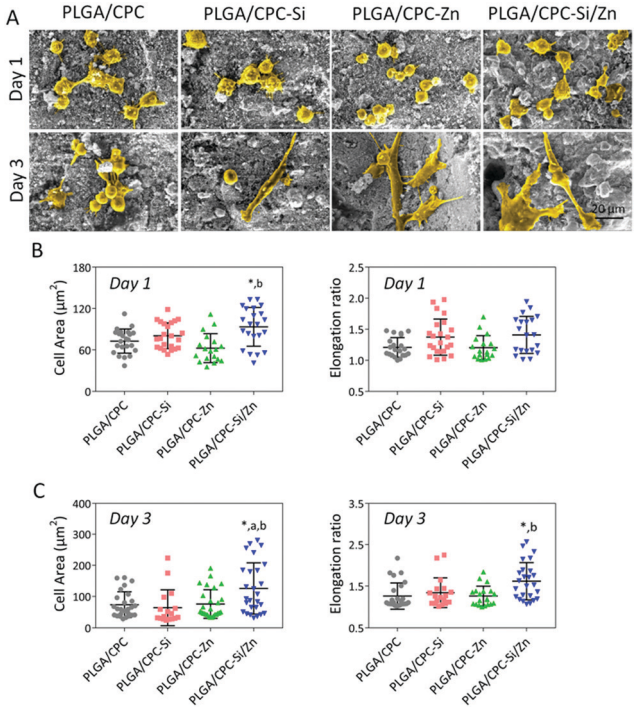

Fig. 4 Morphological changes of RAW 264.7 cells mediated by PLGA/CPC-based scaffolds. (A) SEM images of RAW 264.7 cells cultured on scaffolds for 1 and 3 days. (B) Cell areas and cell elongation ratio after 1 day of co-culture. (C) Cell areas and cell elongation ratio at 3 days of co-culture. In (B and C), symbols represent individual cells ($n = 24$). * Indicates statistically significant difference ($p < 0.05$) compared to the PLGA/CPC group. Statistically significant differences between other groups are indicated with letters (a and b) where 'a' and 'b' indicate significant difference ($p < 0.05$) compared to PLGA/CPC-Si and PLGA/CPC-Zn respectively.

2.4 Osteoimmunomodulatory effects of culture medium conditioned by PLGA/CPC-Si/Zn scaffolds *in vitro*

To investigate whether the immuno-modulatory function of PLGA/CPC-Si/Zn scaffolds can exert pro-osteogenic effects *in vitro*, conditioned media were collected from RAW macrophages cultured on scaffolds to evaluate their effects on the osteogenic differentiation of rBMSCs. Immunofluorescence analysis showed significantly higher production of BMP-2 in the PLGA/CPC-Si/Zn group, as compared to the other groups (Fig. 6A and B) after 3 and 7 days of culture ($p < 0.05$), which was confirmed by the quantitative analysis of fluorescence intensity results (Fig. 6C). A similar trend was also observed at the gene expression level with the RT-qPCR result (Fig. 6D).

2.5 Bone regeneration mediated by PLGA/CPC-Si/Zn scaffolds *in vivo*

As evidenced by micro-CT detection, obvious new bone formation around the implanted trace element incorporated scaffolds were observed after 4 weeks (Fig. 7A), while less new bone formation was observed around the non-incorporated PLGA/CPC scaffold.

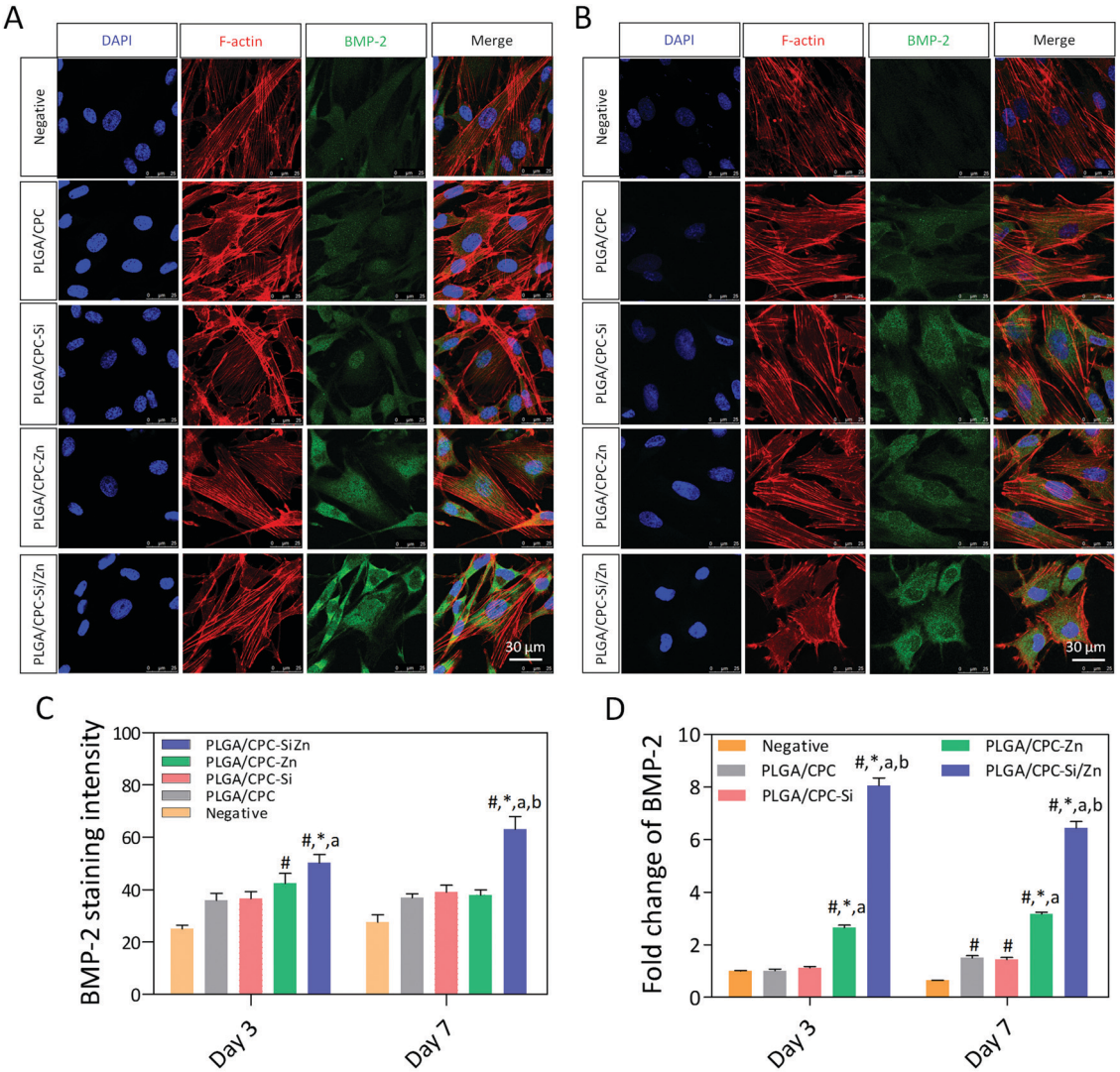

Fig. 6 Osteoimmunomodulatory effects of culture medium conditioned by PLGA/CPC-based scaffolds *in vitro*. Immunofluorescence staining images of rBMSCs cultured on PLGA/CPC-based materials on day 3 (A) and day 7 (B). In the IF images, green represents BMP-2, red represents F-actin and blue represents the cell nuclei. (C) Semi-quantitative analysis of the relative protein expression levels of BMP-2 after 3 and 7 days of culture. (D) mRNA expression levels of BMP-2 in rBMSCs cultured on PLGA/CPC-based materials for 3 and 7 days. # Indicates statistically significant difference ($p < 0.05$) compared to the negative control group. * Indicates statistically significant difference ($p < 0.05$) compared to the PLGA/CPC group. Statistically significant differences between other groups are indicated with letters (a and b) where 'a' and 'b' indicate significant difference ($p < 0.05$) compared to PLGA/CPC-Si and PLGA/CPC-Zn respectively.

As expected, micro-CT analysis showed that the PLGA/CPC-Si/Zn scaffolds yielded a substantial increase in the amount of regenerated bone volume (Fig. 7D). Interestingly, conspicuous new bone ingrowth within the central region of the PLGA/CPC-Si/Zn scaffold could be observed as early as 4 weeks post-implantation from the cross-sectional micro-CT image (in-set in Fig. 7A). However, almost no obvious new bones were seen within the central region of the scaffold material in the other three groups.

Histological analysis further revealed that the PLGA/CPC-Si/Zn scaffolds enhanced conspicuous new bone formation within 4 weeks, and the newly-formed bone tissue could be observed around the PLGA microspheres, together with obvious neovascularization from the Masson staining image (Fig. 7B and C). In contrast, less or no obvious new bone formation were observed in the single element-incorporated and non-incorporated scaffolds. The residual material areas significantly decreased in the PLGA/CPC-Si/Zn group compared to single element-incorporated and non-incorporated groups (Fig. 7E). After 12 weeks of implantation, the PLGA microsphere area was filled with newly-regenerated bone (Fig. 8A) that became partially mature (Fig. 8B) in the PLGA/CPC-Si/Zn group, whereas there was observed to be partially immature new bone continued growing into the PLGA microspheres in the other groups (Fig. 8A and B).

To further investigate the bone regeneration efficacy and degradation performance of the PLGA/CPC-Si/Zn scaffold, the observation time was extended to 24 weeks after implantation. It can be observed that almost all of the PLGA microspheres were uniformly dispersed in the PLGA/CPC-Si/Zn scaffold and

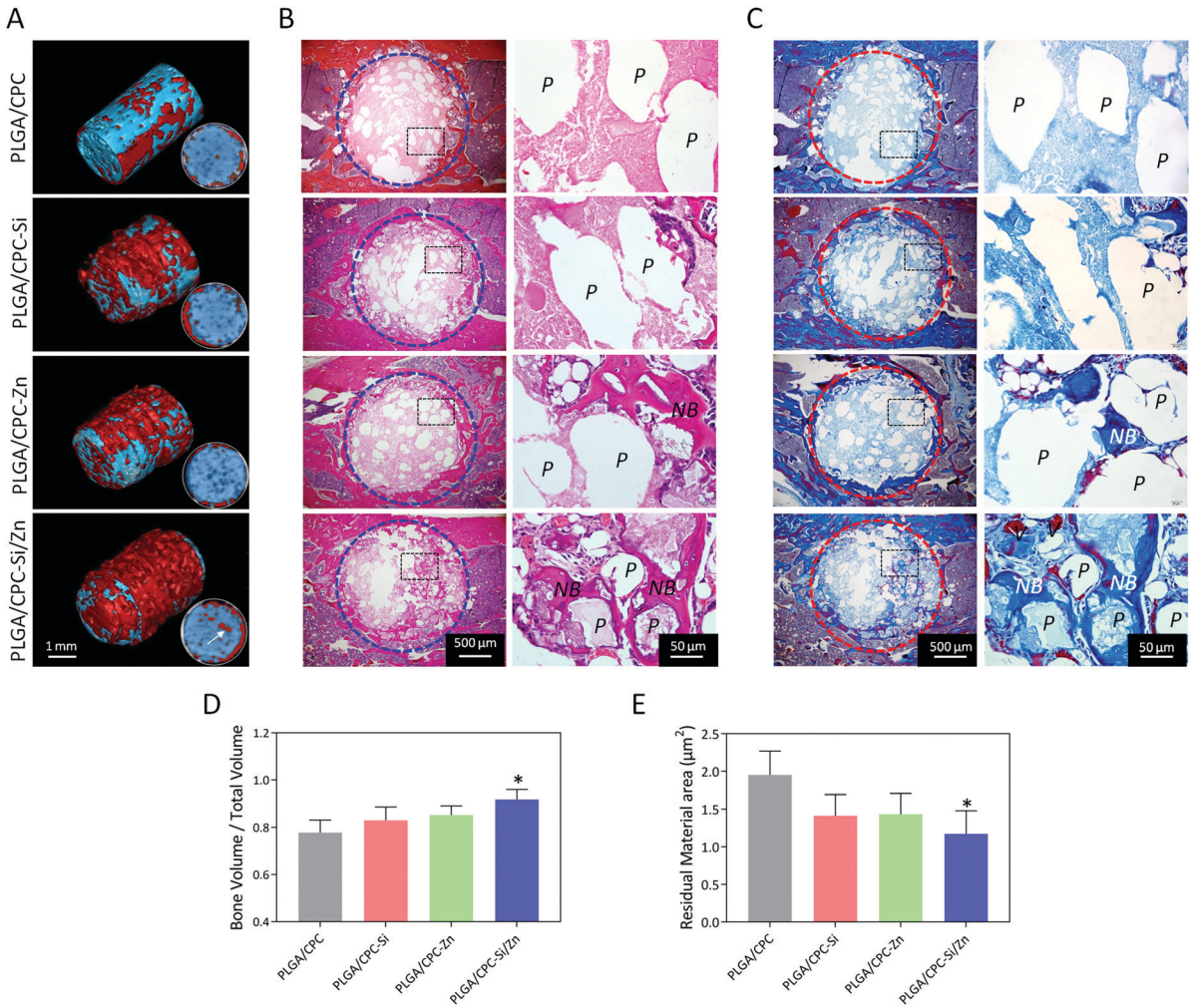

Fig. 7 Bone regeneration in a cavity defect after 4 weeks of implantation of PLGA/CPC-based scaffolds within the rat femur. (A) Three-dimensional reconstruction images (red: new bone formed; blue: material residue. Insets show the cross-sectional micro-CT images. The white arrow denotes the regenerated new bone within the central region of the implanted materials). (B) H&E staining of histological sections. (C) Masson's trichrome staining of histological sections. (P: PLGA microspheres, NB: nascent bone, V: blood vessel. Blue or red dotted frame denote the bone defect site). (D) Quantitative analysis of the ratio of the bone volume to the total volume. (E) Quantitative analysis of residual material areas (*$p < 0.05$, compared with the PLGA/CPC group).

replaced with the newly-regenerated bone (Fig. 9A), with obvious formation of the bone lacuna and bone marrow cavity being observed (Fig. 9B). In addition, the newly formed bone around and inside the PLGA microspheres were combined to form a continuous trabecular bone-like structure (Fig. 9C). Throughout the duration of *in vivo* implantation of the PLGA/CPC-Si/Zn scaffolds, it was observed that there was obvious degradation of the implant material and gradual replacement of the PLGA microspheres with regenerated new bone, as indirectly reflected by the residual material area results (Fig. 9D).

3. Discussion

This study attempted to integrate the osteoinductive potential of Si–Zn dual elements with biodegradable PLGA microspheres in CPC scaffolds. Not only is the release of both Si and Zn ions an improvement over previous studies that focused on single element incorporation, but of greater advantage and novelty is the differential sequential release of Si and Zn ions from our newly-developed scaffold. Because Si ions are released at a faster rate than Zn ions, it might initially promote angiogenesis as reported in a previous study.[21] This was confirmed by our results that showed higher expression levels of vascular markers VEGF and PDGF-BB in macrophages being promoted by either the PLGA/CPC-Si or PLGA/CPC-Si/Zn scaffold, which in turn synergizes with the pro-osteogenic effects of Zn ions.[22] Additionally, improved biodegradability of the CPC scaffolds through incorporation of PLGA microspheres, facilitates the controlled and sustained release of both Si and Zn ions. During the early phase of bone repair, the incorporated PLGA microspheres provide much required mechanical strength to the scaffold, while their degradation during the later phase of bone repair enables increased porosity, which facilitates nutrient/waste transport, cell infiltration and bone ingrowth.[23,24]

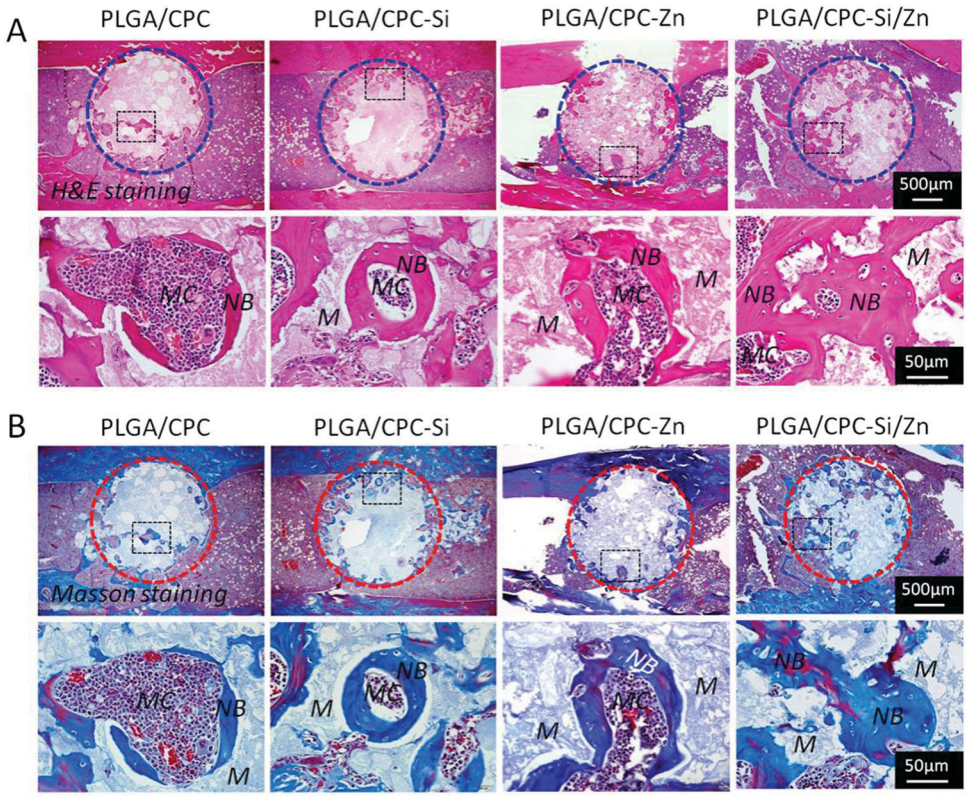

Fig. 8 Bone regeneration in a cavity defect after 12 weeks of implantation of PLGA/CPC-based scaffolds in the rat femur. (A) H&E staining images of the defect sites. (B) Masson's trichrome staining images. The lower images are the enlargement of specific regions of the upper images. (M: material, NB: nascent bone, MC: marrow cavity. Blue or red dotted frame denote the bone defect site).

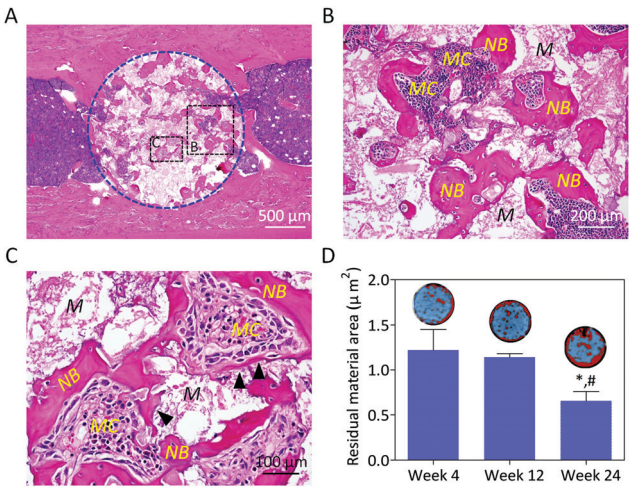

Fig. 9 Bone regeneration in a cavity defect after 24 weeks of implantation of PLGA/CPC-Si/Zn scaffold within the rat femur. (A) H&E staining images of the defect sites (M: material, NB: nascent bone, MC: marrow cavity). (B and C) H&E staining images of the enlargement of specific regions of (A). (D) The analyzed results of residual material areas. Insets show the cross-sectional micro-CT images (red: new bone formed; blue: material residue). (*$p < 0.05$, compared with the week 4 group. #$p < 0.05$, compared with the week 12 group).

The physicochemical properties of CPC scaffolds are critical for their biological functions and clinical applications.[25] In this study, the uniform distribution of the incorporated Si/Zn trace elements and PLGA microspheres could be observed within the CPC scaffolds, which may play a key role in determining the mechanical properties and curing characteristics of the composite scaffolds. Interestingly, the initial setting time and final setting time were significantly prolonged after Si/Zn dual-element doping. Pro-longed setting time has the advantage of allowing material shape correction in adjusting to the actual sizes of bone defects, particularly in complicated cases.[26] The increase of curing time for PLGA/CPC-Si/Zn scaffolds may be due to the fact that zinc silicate does not participate in the hydration of CPC. Moreover, the zinc silicate powder is relatively fine, and its dispersion in CPC causes some hindrance to the hydration reaction. The improved injectability may be explained by the zinc silicate powder having a relatively finer particle size than CPC, which improves the fluidity and stability of the paste. The increase in compressive strength may be attributed to a certain particle dispersion enhancement effect of the zinc silicate particles.[27,28] On the other hand, due to dissolution of silicon ions during the hydration process, the hydration crystallization becomes smaller in size, while the quantity increases, thereby improving the mechanical strength of the overall material. These findings thus suggest that the incorporation of Si/Zn dual-elements could be beneficial for improving some of the key properties of CPC scaffolds for clinical applications including the setting time, injectability and compressive strength of the scaffolds.

The controlled release kinetics of trace elements are critical for bone regeneration.[29] In this study, the release profiles of Si and Zn ions in all scaffold groups exhibited an initial burst release,

followed gradually by a sustained release state. The initial burst release of trace elements is beneficial for bone regeneration, as demonstrated by a previous study, which showed that the quickly-released trace elements from the scaffold material can act as a chemical signal to induce cytokines to stimulate proliferation and osteogenic differentiation of stem cells.[30] Subsequent sustained release of trace elements may be related to the degradation of the PLGA microspheres, which provides adequate space for liquid infiltration and elution of ions, according to our previous *in vitro* degradation results.[16] The sustained release of trace elements will help maintain the osteoinductive activity of the scaffold materials and promote bone regeneration.[31,32] The sequential release pattern, in which Si was released faster than Zn, may be due to Zn participating in the hydration process of bone cement, whereas Si was released earlier, as it did not participate in the hydration process. Silicon has been shown to induce angiogenesis by upregulating nitric oxide synthase (NOS), leading to increased VEGF production,[33] which has also been confirmed by our results that high expression levels of vascular markers VEGF and PDGF-BB in macrophages are promoted by the PLGA/CPC-Si/Zn scaffold. Within the cellular microenvironment, Zn is thought to stop the osteoclastic resorption process and stimulate the osteoblastic bone formation process.[22] Hence, it might be inferred that incorporation of biodegradable PLGA microspheres is beneficial to the sequential release pattern of Si–Zn dual-elements from the PLGA/CPC-Si/Zn scaffold, which facilitates early vascularization and later osteogenesis, correctly orchestrated in accordance with the natural process of bone defect repair.

The osteoimmunomodulatory properties of bone biomaterials are of great importance in determining the bone repair efficacy of the implants.[34,35] Trace element incorporation is an important strategy to optimize the osteoimmunomodulatory properties of implant materials, because trace elements are essential for proper functioning of the immune system.[36–38] The Si-containing ionic products released from silicate bioceramics have been shown to inhibit the macrophage inflammatory responses *via* suppression of the activated NF-κB signaling pathway and promoting the caspase-dependent apoptosis of macrophages.[9] Zn^{2+} is a second messenger for signal transduction in immune cells and can suppress osteoclastogenesis through antagonism of either NF-κB signaling[39] or the TLR-4 pathway.[40] In this study, we found that the PLGA/CPC-Si/Zn scaffold exhibited the most potent anti-inflammatory effects as compared to single-element incorporated or non-incorporated scaffolds. This suggests that the dual-element release of Si and Zn ions has a synergistic regulatory effect on inflammatory responses. BMSCs exposed to the conditioned medium of macrophage cultured on the PLGA/CPC-Si/Zn scaffold exhibited the highest expression of BMP-2, as compared to the other scaffold groups. This is likely due to the synergistic effects of Si/Zn ions released from the PLGA/CPC-Si/Zn scaffold on osteoblast activity,[41] as well as their positive anti-inflammatory and pro-angiogenic effects on macrophages.[42] These results demonstrate that the PLGA/CPC-Si/Zn scaffold can exert an integrated osteoimmunomodulatory effect that significantly enhance bone repair efficacy by creating a favorable microenvironment upon implantation into bone defects.

For any bone substitute material, there must be a fine balance between degradation of the implanted material and its effective replacement by new bone tissue, to achieve optimal efficacy in bone defect repair.[43] In this study, incorporation of PLGA microspheres and Si/Zn duel-elements within the CPC scaffolds led to obvious new bone formation after 4 weeks post-implantation within rat femur defects. This may be attributed to the potential osteoimmunomodulatory property of the scaffolds resulting from sustained and sequential release of Si/Zn ions. Additionally, the positive bone regenerative outcome may also be attributed to the pro-angiogenic effects of the PLGA/CPC-Si/Zn scaffold, which was confirmed by the Masson staining results *in vivo* and vascular gene marker analysis results *in vitro*.

Subsequently at 12 weeks post-implantation, the apparent bone ingrowth into the PLGA microspheres resulted in the scaffold being almost completely filled with mature new bone. Full degradation of the PLGA micro-spheres at 24 weeks can be attributed to hydrolysis from body fluids and physicochemical dissolution by Si/Zn ions.[44–46] Taken together, these findings thus indicate that the PLGA/CPC-Si/Zn scaffolds can accelerate the bone repair process through the synergy of dual-element incorporation with improved biodegradability endowed by PLGA microspheres incorporation.

4. Experimental

4.1 Synthesis and preparation of CPC powders and PLGA microspheres

CPC powders used in this work were a mixture of partially crystallized calcium phosphate (PCCP) and anhydrous dicalcium phosphate (DCPA, CaHPO4) at a mass ratio of 1 : 1 as developed in our previous work.[16] PLGA microspheres were made by a solvent evaporation method. Briefly, PLGA (50/50 lactide to glycolic acid ratio, mol. wt. = 30 000) was dissolved in methylene chloride (CH_2Cl_2) to form a homogeneous solution, which was subsequently syringed into 0.1 g L^{-1} vinyl alcohol solution. The solution was stirred at 450 rpm with an overhead stirrer for 8 h at room temperature, allowing the solvent to evaporate. After stirring, the solution was allowed to stand for 4 h and the liquid was decanted. The microspheres were then washed three times with deionized water, centrifuged and lyophilized. The microspheres were sieved in the range of 50–200 μm and stored at −20 °C.

4.2 Preparation of PLGA/CPC scaffolds incorporated with Si and/or Zn elements

The samples were divided into four groups according to the incorporated trace element: (1) PLGA/CPC group as control, without any trace element; (2) PLGA/CPC-Si group, containing silicon within CPC through incorporation of calcium silicate ($CaSiO_3$). $CaSiO_3$ powder was synthesized by the chemical precipitation method. Sodium metasilicate nona-hydrate ($Na_2SiO_3{\cdot}9H_2O$) and calcium chloride ($CaCl_2$) were used as the source of Si and Ca.[47] (3) PLGA/CPC-Zn group, containing zinc in CPC through incorporation of Zn incorporated-tricalcium phosphate (Zn-TCP). Zn-TCP was synthesized by a high-temperature solid-state reaction

using commercially-available calcium dihydrogen phosphate ($CaHPO_4{\cdot}2H_2O$), calcium carbonate ($CaCO_3$), and zinc acetate ($Zn(CH_3COO)_2$). Briefly, the chemical reagents were mixed in ethanol with (Ca + Zn)/P molar ratio of 3 : 2 and milled into a homogeneous slurry using a planet ball mill (250 rpm for 2 h). The slurry was oven-dried at 80 °C for 24 h and calcined in a muffle furnace at 1000 °C for 2 h. Finally, Zn-TCP powder with a particle size of less than 106 μm were obtained by sieving with an oscillating sieving machine. (4) PLGA/CPC-Si/Zn group, containing silicon and zinc within CPC through incorporation of zinc silicate (Zn_2SiO_4). Zn_2SiO_4 was synthesized by the hydrothermal method (170 °C, 6 h) as reported in our previous study.[48]

All powders of each group were mixed uniformly by dry-grinding in a ball mill for 24 h. The blended powders were homogeneously mixed with deionized water at a powder to liquid ratio of 0.35 g ml^{-1}. After pouring the cement into the steel molds, the cement was pressed by a steel column with a diameter of 10.0 mm under a stress of about 700 kPa for 5s to eliminate the big air bubbles. The pastes were maintained for three days at 37 °C and a humidity of 90–95% within a CO_2 incubator, and then dried at 50 °C for 24 h. The chemical composition of the various PLGA/CPC-based materials was presented in Table 1.

4.3 Physicochemical characterization of PLGA/CPC-Si/Zn composite scaffolds

The cross-sectional microstructure of the PLGA/CPC-Si/Zn scaffold was imaged with SEM (ZEISS Ultra 55, Germany). The distribution of trace elements was characterized by an energy dispersive spectrometer (EDS). The phase composition and group contents were analyzed by X-ray diffraction analysis (XRD; D8 Advance, Japan). The compressive strength of the cements was measured by a universal material testing machine (Instron 5567, Instron, USA) and the final presented data of each group was the average value of six duplicate reading. The setting time of cements was measured according to the Gilmore needle method.[49] Injectability of the cements was tested using a syringe, which was fitted with a needle of 2.1 mm in inner diameter. The porosity of PLGA/CPC-based materials was measured by the Archimedes method.[23] The samples (3 pieces each group) were immersed within the phosphate buffer solution (PBS) and kept at 37 °C for defined time periods (0, 2, 4, 6, 8, 10, 12, 14, 21, 28 days). The ionic concentrations of Si and Zn released by PLGA/CPC-based materials in the buffer solution were tested by inductively coupled plasma atomic emission spectroscopy (ICP-AES, Varian 715 ES, California, USA). The ion concentration of every time point was tested as Cn and the cumulative release percentage (Tn) was calculated by the equation of Tn (%) = (C1 + C2 + …Cn)/(C1 + C2 + …C10) × 100.

4.4 Cell culture

The murine-derived macrophage cell line RAW 264.7 and rat bone marrow mesenchymal stem cells (BMSCs) were utilized in this study. RAW 264.7 cells were cultured in Dulbecco's Modified Eagle Medium (DMEM, Life Technologies, Carlsbad, California, USA) supplemented with 10% (v/v) fetal bovine serum (FBS, Thermo Scientific, Australia) and 1% (v/v) penicillin/streptomycin (Life Technologies, Carlsbad, California, USA) within a humidified CO_2 incubator at 37 °C. RAW 264.7 cells were passaged at approximately 80% confluence by scraping. Rat BMSCs (Cyagen Biosciences, Inc., China) were routinely maintained in mesenchymal stem cell basal medium supplemented with 10% (v/v) FBS, 1% (v/v) penicillin/streptomycin and 2 mM glutamine (Cyagen Biosciences, Inc., China) at 37 °C within a humidified CO_2 incubator. Cells were utilized for further experiments after two passages.

4.5 Morphological observation of RAW 264.7 cells on composite scaffolds

RAW 264.7 cells were seeded on the various scaffolds at a density of 2×10^5 ml^{-1}. The cell morphology on the various scaffolds was observed with SEM. After culture for 1 and 3 days, the samples were washed three times with PBS, fixed in 2.5% (w/v) glutaraldehyde, incubated with 0.18 mol L^{-1} sucrose and dehydrated through a graded ethanol series (30–100%), followed by air drying. SEM images were analyzed by a semiautomatic image analysis system (Image pro plus 6.0) and pseudo-colored by Photoshop. Additionally, image analysis was performed to quantify the spreading area and elongation ratio (n = 24) of RAW 264.7 cells.

4.6 M1 and M2 surface markers changes of RAW 264.7 cells

Expression of the macrophage surface markers CCR7 (M1) and CD206 (M2) were estimated by flow cytometry. RAW 264.7 cells were seeded on different samples at a density of 1×10^6 cells per well (6-well plate). After 1 and 3 days of culture, the cells were detached by cell scrapers, fixed with 4% (w/v) paraformaldehyde (PFA) for 30 min, and treated with 3% (v/v) BSA to block non-specific antigen binding. The samples were incubated with CCR7 antibody (ab95669, Abcam) and CD206 antibody (ab195192, Abcam) for 60 min at 4 °C. After washing with 1% (w/v) BSA, the expression was analyzed on a flow cytometer (BD Biosciences). The percentages of positively-stained cells were determined and compared.

4.7 Gene expression and cytokine secretion by RAW 264.7 cells cultured on composite scaffolds

RAW 264.7 cells were seeded on composite scaffolds (n = 4) at a density of 5×10^5 cells per well (6-well plate). After 3 days of culture, total RNA was harvested using TRIzol reagent (Invitrogen, USA). Complementary DNA was synthesized from 1000 ng of total

Table 1 Chemical composition of PLGA/CPC-based scaffold materials

Group	CPC (wt%)	DCPA (wt%)	PLGA (wt%)	$CaSiO_3$ (wt%)	Zn-TCP (wt%)	Zn_2SiO_4 (wt%)
PLGA/CPC	42.5	42.5	15	0	0	0
PLGA/CPC-Si	41.2	41.2	15	2.6	0	0
PLGA/CPC-Zn	35	35	15	0	15	0
PLGA/CPC-Si/Zn	40	40.5	15	0	0	5

Table 2 Primer sequences of inflammatory gene markers utilized in RT-qPCR

Genes	Primer sequences
GAPDH	Forward: 5′-CATCTTCCAGGAGCGAGACC-3′ Reverse: 5′-CTCGTGGTTCACACCCATCA-3′
IL-10	Forward: 5′-GCATGGCCCAGAAATCAAGG-3′ Reverse: 5′-GAGAAATCGATGACAGCGCC-3′
PDGF-BB	Forward: 5′-ACTTGAACATGACCCGAGCACA-3′ Reverse: 5′-GCATTGCACATTGCGGTTATT-3′
VEGF	Forward: 5′-CGATTGAGACCCTGGTGGACA-3′ Reverse: 5′-GTGAGGTTTGATCCGCATGATC-3′
TGF-1β	Forward: 5′-CAGTACAGCAAGGTCCTTGC-3′ Reverse: 5′-ACGTAGTAGACGATGGGCAG-3′
TNF-α	Forward: 5′-AAGAGGCACTCCCCCAAAAG-3′ Reverse: 5′-GCTACAGGCTTGTCACTCGAA-3′

Table 3 Primer sequences of bone-related gene markers utilized in RT-qPCR

Genes	Primer sequences
GAPDH	Forward: 5′-GGTCGGTGTGAACGGATTTGG-3′ Reverse: 5′-GCCGTGGGTAGAGTCATACTGGAAC-3′
BMP-2	Forward: 5′-TGCTCAGCTTCCATCACGAAG-3′ Reverse: 5′-TCTGGAGCTCTGCAGATGTGA-3′

RNA using the reverse transcription system (Takara, Japan). The primer sequences used for gene expression analysis are listed in Table 2. The mRNA expression of pro-inflammatory gene (TNF-α), anti-inflammatory genes (IL-10 and TGF-1β) and vascular genes (VEGF and PDGF-BB) was assayed on the ABI Prism 8000 Thermal Cycler (Applied Biosystems, USA) using SYBR Green qPCR Master Mix reagent (Roche, Switzerland). Relative gene expression was normalized against expression of the house-keeping GAPDH.

For ELISA analysis, RAW 264.7 cells were seeded on the scaffolds at a density of 2×10^5 cells per ml. After 1 and 3 days, the medium was collected and subjected to centrifugation at 250 g, and the secreted IL-6 within the supernatants was detected by a mouse ELISA kit (eBioscience) following the manufacturer's instruction.

4.8 Effects of RAW 264.7 cell-conditioned medium on the osteogenic differentiation of BMSCs

4.8.1 Immunofluorescence staining. RAW 264.7 cells were seeded on different samples at a density of 1×10^6 cells per well (6-well plate). After 3 days, the medium was collected and subjected to centrifugation at 250 g and the supernatants were mixed with normal culture medium at a ratio of 1 : 2 and stored at −80 °C for conditioned medium experiments. Rat BMSCs were plated at a density of 5×10^4 cells per well in 24-well plates. After 24 h of incubation, the culture medium was removed and replaced with conditioned or control medium. After culture for 3 and 7 days, the cells were fixed with 4% (w/v) PFA for 30 min, permeabilized with 0.1% (w/v) Triton X-100 for 10 min, and blocked with 3% (w/v) BSA for 1 h at room temperature. Samples were incubated with primary antibodies against BMP-2 (ab14933, Abcam) in 1% (w/v) BSA overnight at 4 °C. After washing off the primary antibody, the samples were incubated with the secondary antibody (ab150083, Abcam) for 1 h at room temperature. Then cells were treated with Phalloidin-TRITC (Sigma) for 1 h and then stained with DAPI (Roche) for 10 min at room temperature. Images were captured under confocal microscopy (Leica Microsystem, Germany). Additionally, image analysis was performed to quantify the fluorescence intensity of rat BMSCs. Measurements were performed on a minimum of 20 cells in each group.

4.8.2 Real-time PCR assay. Rat BMSCs were seeded in 6-well plates ($n = 4$) at a density of 2×10^5 cells per well. After 24 h of incubation, the culture medium was removed and replaced with conditioned or control medium. After culturing for 3 and 7 days, total RNA was extracted from each sample using TRIZOL reagent (Invitrogen, USA) following the manufacturer's instructions. The RNA was then reverse transcribed into cDNA using the reverse transcription system (Takara, Japan). Real-time PCR was performed by using the SYBR Green detection system with an ABI PRISM 8000 Real-Time PCR system (Roche, Switzerland). All reactions were carried out in triplicates. The primer sequences of osteogenic gene markers are listed in Table 3.

4.9 Animals and surgical procedures

A total of 38 male Sprague-Dawley rats (8-weeks old) were used in this study. The experimental protocol was approved by the Animal Care and Use Committee of Peking University. All the rats were randomly divided into four groups corresponding to PLGA/CPC, PLGA/CPC-Si, PLGA/CPC-Zn and PLGA/CPC-Si/Zn. Firstly, the rats were anesthetized by intraperitoneal injection of 40 mg kg^{-1} pentobarbital sodium. Surgical equipment was used to make a cylindrical defect with diameter of 2 mm and height of 5 mm. After removing the necessary bone mass, the scaffolds with diameter of 2 mm and height of 5 mm were implanted into the defect and the muscular fascia, subcutaneous tissue and skin were sutured in sequence. Two femurs of each rat were implanted with different scaffolds and each scaffold group had at least 3 replicates at every timepoint. The rats were sacrificed after implantation of 4, 12 and 24 weeks. The femurs were then detached from the rats and fixed in 10% (v/v) neutral buffered formalin, prior to further processing for histological analysis.

4.10 Micro-CT evaluation

The harvested femurs were examined using micro-CT scanning (INVEON MM GANTRY-S, SIEMENS). The Micro-CT measurement was performed using a monochromatic beam with a voltage of 80 kV and a current of 500 mA and scanning along the long axis of the specimen. The images were reconstructed by supporting software (Inveon Research Workplace). The 3D reconstructed images were further analyzed to evaluate bone regeneration effects of implanted materials *in vivo* in term of bone volume-to-total volume ratio.

4.11 Histological analysis

Tissue processing and sectioning were performed as previously described.[50] Briefly, tissue samples were fixed in 10% (w/v) neutral buffered formalin, decalcified and dehydrated, embedded in paraffin, and sectioned at a thickness of 5 μm. H&E staining and Masson's trichrome staining were then carried out respectively on

the tissue sections, according to the manufacturers' recommended protocols, and images were captured under light microscopy (Olympus, Japan). Histological parameters were measured with a microscope (Leica Mtla, German). A supporting software (Bioquant Osteo Bone Biology Research System) was used to measure the surfaces of sections and obtain residual areas of CPC-based materials.

4.12 Statistical analysis

All quantitative data were expressed as mean ± standard deviation. Statistical analysis was performed using the SPSS 19.0 software (Chicago, IL). Differences between data sets were analyzed using one-way analysis of variance (ANOVA). A value of $p < 0.05$ was assumed to be statistically significant.

5. Conclusions

In summary, a novel PLGA microsphere-containing CPC scaffold co-incorporated with two trace elements – silicon and zinc (PLGA/CPC-Si/Zn) was fabricated and the effects of this composite scaffold on mechanical properties, trace element release kinetics, immune responses and osteogenesis were evaluated. The incorporation of Si/Zn dual-elements improved the setting time, injectability and compressive strength of the scaffolds. The controllable and sequential release of Si and Zn is evident in the PLGA/CPC-Si/Zn scaffolds. *In vitro*, PLGA/CPC-Si/Zn scaffolds significantly enhanced the anti-inflammatory gene expression and M2 phenotype transformation of macrophages. Additionally, the PLGA/CPC-Si/Zn scaffolds can also exert a systemic osteoimmunomodulatory effect on rat BMSCs *in vitro* and significantly enhance bone regeneration *in vivo*, suggesting that the combinatorial effects of PLGA microspheres and Si/Zn dual-elements incorporation within the CPC scaffolds synergistically enhanced bone regeneration.

Conflicts of interest

There are no conflicts to declare.

Acknowledgements

This work was supported by the National Key R&D Program of China (2018YFC1105303/04, 2017YFC1104302/03), National Natural Science Foundation of China (No. 51772006, 81425007, 31670993, 51973004), Beijing Municipal Science & Technology Commission Project (Z181100002018001).

References

1 Y. Zhou, C. Wu and J. Chang, *Mater. Today*, 2019, **24**, 41–56.
2 A. Wubneh, E. K. Tsekoura, C. Ayranci and H. Uludağ, *Acta Biomater.*, 2018, **80**, 1–30.
3 S. Bose, G. Fielding, S. Tarafder and A. Bandyopadhyay, *Trends Biotechnol.*, 2013, **31**, 594–605.
4 S. H. Lin, W. J. Zhang and X. Q. Jiang, *Chin. J. Dent. Res.*, 2019, **22**, 93–104.
5 W. Götz, E. Tobiasch, S. Witzleben and M. Schulze, *Pharmaceutics*, 2019, **11**, 1–27.
6 W. Zhang, D. Huang, F. Zhao, W. Gao, L. Sun, X. Li and X. Chen, *Mater. Sci. Eng., C*, 2018, **89**, 245–255.
7 A. Ilyas, M. Velton, A. Shah, F. Monte, H. K. W. Kim, P. B. Aswath and V. G. Varanasi, *J. Biomed. Nanotechnol.*, 2019, **15**, 1241–1255.
8 G. A. Fielding, W. Smoot and S. Bose, *J. Biomed. Mater. Res., Part A*, 2014, **102**, 2417–2426.
9 Y. Huang, C. Wu, X. Zhang, J. Chang and K. Dai, *Acta Biomater.*, 2018, **66**, 81–92.
10 A. S. Tiffany, D. L. Gray, T. J. Woods, K. Subedi and B. A. C. Harley, *Acta Biomater.*, 2019, **93**, 86–96.
11 M. Shi, Z. Chen, S. Farnaghi, T. Friis, X. Mao, Y. Xiao and C. Wu, *Acta Biomater.*, 2016, **30**, 334–344.
12 C. Wu, Z. Chen, Q. Wu, D. Yi, T. Friis, X. Zheng, J. Chang, X. Jiang and Y. Xiao, *Biomaterials*, 2015, **71**, 35–47.
13 M. Wang, Y. Yu, K. Dai, Z. Ma, Y. Liu, J. Wang and C. Liu, *Biomater. Sci.*, 2016, **4**, 1574–1583.
14 A. J. Ambard and L. Mueninghoff, *J. Prosthodontics*, 2006, **15**, 321–328.
15 J. Zhang, W. Liu, V. Schnitzler, F. Tancret and J. M. Bouler, *Acta Biomater.*, 2014, **10**, 1035–1049.
16 X. Qi, J. Ye and Y. Wang, *Acta Biomater.*, 2008, **4**, 1837–1845.
17 F. He, Y. Chen, J. Li, B. Lin, B. Yu, Y. Ouyang, Y. Xia, B. Yu and J. Ye, *J. Biomed. Mater. Res., Part A*, 2015, **103**, 1312–1324.
18 S. Arabnejad, R. Burnett Johnston, J. A. Pura, B. Singh, M. Tanzer and D. Pasini, *Acta Biomater.*, 2016, **30**, 345–356.
19 P. J. Murray, *Annu. Rev. Physiol.*, 2017, **79**, 541–566.
20 D. M. Mosser and J. P. Edwards, *Nat. Rev. Immunol.*, 2008, **8**, 958–969.
21 F. Monte, T. Cebe, D. Ripperger, F. Ighani, H. V. Kojouharov, B. M. Chen, H. K. W. Kim, P. B. Aswath and V. G. Varanasi, *J. Tissue Eng. Regener. Med.*, 2018, **12**, 2203–2220.
22 K. B. Hadley, S. M. Newman and J. R. Hunt, *J. Nutr. Biochem.*, 2010, **21**, 297–303.
23 T. Wu, H. Shi and J. Ye, *RSC Adv.*, 2015, **5**, 47749–47756.
24 R. P. Félix Lanao, S. C. G. Leeuwenburgh, J. G. C. Wolke and J. A. Jansen, *Biomaterials*, 2011, **32**, 8839–8847.
25 I. Palmer, J. Nelson, W. Schatton, N. J. Dunne, F. J. Buchanan and S. A. Clarke, *J. Biomed. Mater. Res., Part B*, 2016, **104**, 308–315.
26 L. Ambrosio, V. Guarino, V. Sanginario, P. Torricelli, M. Fini, M. P. Ginebra, J. A. Planell and R. Giardino, *Biomed. Mater.*, 2012, **7**, 024113.
27 M. Looney, H. O. Shea, L. Gunn, D. Crowley and D. Boyd, *J. Biomater. Appl.*, 2013, **27**, 937–947.
28 M. S. Hasan, S. Kehoe and D. Boyd, *J. Biomater. Appl.*, 2014, **29**, 566–581.
29 S. Ali Akbari Ghavimi, R. R. Tata, A. J. Greenwald, B. N. Allen, D. A. Grant, S. A. Grant, M. W. Lee and B. D. Ulery, *AAPS J.*, 2017, **19**, 1029–1044.
30 T. Odatsu, T. Azimaie, M. F. Velten, M. Vu, M. B. Lyles, H. K. Kim, P. B. Aswath and V. G. Varanasi, *J. Biomed. Mater. Res., Part A*, 2015, **103**, 2797–2806.
31 K. Zhang, S. Lin, Q. Feng, C. Dong, Y. Yang, G. Li and L. Bian, *Acta Biomater.*, 2017, **64**, 389–400.

32 S. Zhang, Q. Liu, L. Li, Y. Bai and B. Yang, *Mater. Sci. Eng., C*, 2018, **93**, 1027–1035.
33 H. Li, K. Xue, N. Kong, K. Liu and J. Chang, *Biomaterials*, 2014, **35**, 3803–3818.
34 K. Okamoto, T. Nakashima, M. Shinohara, T. Negishi-Koga, N. Komatsu, A. Terashima, S. Sawa, T. Nitta and H. Takayanagi, *Physiol. Rev.*, 2017, **97**, 1295–1349.
35 M. C. Walsh, N. Kim, Y. Kadono, J. Rho, S. Y. Lee, J. Lorenzo and Y. Choi, *Annu. Rev. Immunol.*, 2006, **24**, 33–63.
36 S. Maggini, E. S. Wintergerst, S. Beveridge and D. H. Hornig, *Br. J. Nutr.*, 2007, **98**, 29–35.
37 P. Verma, A. K. Sharma, H. Shankar, A. Sharma and D. N. Rao, *Biol. Trace Elem. Res.*, 2018, **184**, 325–333.
38 Z. Chen, J. Yuen, R. Crawford, J. Chang, C. Wu and Y. Xiao, *Biomaterials*, 2015, **61**, 126–138.
39 M. Yamaguchi and M. N. Weitzmann, *Mol. Cell. Biochem.*, 2011, **355**, 179–186.
40 C. Kessel, S. Fuehner, J. Zell, B. Zimmermann, S. Drewianka, S. Brockmeyer, D. Holzinger, C. Hinze, H. Wittkowski and D. Foell, *J. Allergy Clin. Immunol.*, 2018, **142**(1370–1373), e8.
41 G. Fielding and S. Bose, *Acta Biomater.*, 2013, **9**, 9137–9148.
42 T. G. Khonina, M. V. Ivanenko, O. N. Chupakhin, A. P. Safronov, E. A. Bogdanova, M. S. Karabanalov, V. V. Permikin, L. P. Larionov and L. I. Drozdova, *Eur. J. Pharm. Sci.*, 2017, **107**, 197–202.
43 J. E. Dumas, E. M. Prieto, K. J. Zienkiewicz, T. Guda, J. C. Wenke, J. Bible, G. E. Holt and S. A. Guelcher, *Tissue Eng., Part A*, 2014, **20**, 115–129.
44 M. L. Houchin and E. M. Topp, *J. Pharm. Sci.*, 2008, **97**, 2395–2404.
45 W. J. E. M. Habraken, J. G. C. Wolke, A. G. Mikos and J. A. Jansen, *J. Biomater. Sci., Polym. Ed.*, 2008, **19**, 1171–1188.
46 E. Fortunati, L. Latterini, S. Rinaldi, J. M. Kenny and I. Armentano, *J. Mater. Sci.: Mater. Med.*, 2011, **22**, 2735–2744.
47 K. Xiong, H. Shi, J. Liu, Z. Shen, H. Li and J. Ye, *J. Am. Ceram. Soc.*, 2013, **96**, 691–696.
48 K. Xiong, J. Zhang, H. Shi, J. Liu, H. Wu, H. Li and J. Ye, *RSC Adv.*, 2015, **5**, 8329–8339.
49 J. Zhang, H. S. Shi, J. Q. Liu, T. Yu, Z. H. Shen and J. D. Ye, *J. Mater. Chem. B*, 2015, **3**, 8782–8795.
50 S. Meng, X. Zhang, M. Xu, B. C. Heng, X. Dai, X. Mo, J. Wei, Y. Wei and X. Deng, Biomed. Mater., 2015, **10**, 035006.